TU Delft

Delft University of Technology

2D V_2C MXene Based Flexible Gas Sensor for Highly Selective and Sensitive Toluene Detection at Room Temperature

Karmakar, Sourav; Deepak, Mavuri Sai; Nanda, Om Priya; Sett, Avik; Maity, Palash Chandra; Karmakar, Gairik; Sha, Rinky; Badhulika, Sushmee; Bhattacharyya, Tarun Kanti

DOI
10.1021/acsaelm.4c00369

Publication date
2024

Document Version
Final published version

Published in
ACS Applied Electronic Materials

Citation (APA)
Karmakar, S., Deepak, M. S., Nanda, O. P., Sett, A., Maity, P. C., Karmakar, G., Sha, R., Badhulika, S., & Bhattacharyya, T. K. (2024). 2D V_2C MXene Based Flexible Gas Sensor for Highly Selective and Sensitive Toluene Detection at Room Temperature. *ACS Applied Electronic Materials*, *6*(5), 3717-3725. https://doi.org/10.1021/acsaelm.4c00369

Important note
To cite this publication, please use the final published version (if applicable).
Please check the document version above.

Copyright
Other than for strictly personal use, it is not permitted to download, forward or distribute the text or part of it, without the consent of the author(s) and/or copyright holder(s), unless the work is under an open content license such as Creative Commons.

Takedown policy
Please contact us and provide details if you believe this document breaches copyrights.
We will remove access to the work immediately and investigate your claim.

This work is downloaded from Delft University of Technology.
For technical reasons the number of authors shown on this cover page is limited to a maximum of 10.

Green Open Access added to TU Delft Institutional Repository

'You share, we take care!' - Taverne project

https://www.openaccess.nl/en/you-share-we-take-care

Otherwise as indicated in the copyright section: the publisher is the copyright holder of this work and the author uses the Dutch legislation to make this work public.

ACS APPLIED ELECTRONIC MATERIALS

pubs.acs.org/acsaelm Article

2D V_2C MXene Based Flexible Gas Sensor for Highly Selective and Sensitive Toluene Detection at Room Temperature

Sourav Karmakar, Mavuri Sai Deepak, Om Priya Nanda, Avik Sett, Palash Chandra Maity, Gairik Karmakar, Rinky Sha,* Sushmee Badhulika,* and Tarun Kanti Bhattacharyya

Cite This: https://doi.org/10.1021/acsaelm.4c00369 Read Online

ACCESS | Metrics & More | Article Recommendations | Supporting Information

ABSTRACT: While the majority of the reports on toluene gas sensors are on rigid electrodes and based on composite materials, doping with additional noble metals, or a high temperature detection method, this work is the first demonstration of the vanadium carbide (V_2C) MXene based flexible and room-temperature (RT) toluene gas sensor. The V_2C MXene is synthesized by an HF etching route. The field emission scanning electron microscopy (FESEM) and transmission electron microscopy (TEM) images exhibit a typical accordion-like multilayered structure of the V_2C MXene, where the Fourier-transform infrared spectroscopy (FTIR), Raman, and X-ray photoelectron spectroscopy (XPS) data further ensured its successful growth. The V_2C (band gap of 3.9 eV) based flexible gas sensor employing a polyester substrate, displays good reproducibility, quick response/recovery time (14 s/34 s), long-term stability, good cross-selectivity, and a low detection limit of 47.85 ppb over the linear region of 5−200 ppm toluene at RT (27 ± 1 °C). The effect of relative humidity (RH) toward RT toluene gas sensing has also been investigated here. This sensor shows an excellent response of 775% at 200 ppm toluene, with brilliant selectivity toward toluene over six other hazardous gases. The sensor's plentiful surface functional groups (−F, −OH, −O) and superior electrical characteristics are responsible for its enhanced performance. In light of this, the flexible and RT toluene gas sensor based on the V_2C MXene can be a smart way to fabricate the next-generation toluene gas sensors.

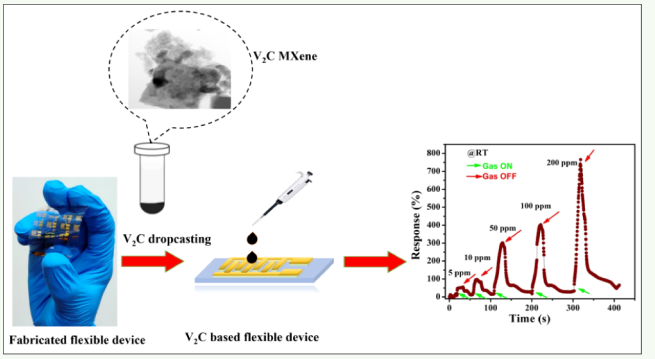

KEYWORDS: *V_2C MXene, gas sensor, room-temperature, toluene, flexible*

Downloaded via TU DELFT on May 23, 2024 at 06:48:31 (UTC).
See https://pubs.acs.org/sharingguidelines for options on how to legitimately share published articles.

1. INTRODUCTION

In conventional gas sensors, rigid materials such as silicon, glass, etc. have been extensively used as a substrate. Major drawbacks associated with these types of gas sensors are their bulkiness, high operating temperature, and complexity in nature.[1,2] To overcome these drawbacks, flexible gas sensors have recently gained considerable attention among the research communities for their usage in wearable electronics like smartwatches, bands, human skins, robots, and so on because of their attractive properties, including low-cost, lightweight, compactness, and real-time monitoring of toxic gases without any requirement of special conditions.[3,4] Flexible gas sensors are usually made up of electrodes, sensing materials, and a flexible substrate. Paper, polyethylene naphthalate, poly(ethylene terephthalate) (PET), polyimide, poly(dimethylsiloxane), polyester film, etc., are the substrates that are most often employed because of their unique properties such as biocompatibility, portability, flexibility, and so forth.[5,6] The chemiresistive-based flexible gas sensors have been widely utilized to detect various harmful gases like ammonia (NH_3), nitrogen dioxide (NO_2), and volatile organic compounds (VOCs) at room temperature (RT).[7−11]

Toluene, a colorless, toxic VOC, is mainly emitted by automobiles and the farming sector. It is also utilized as an organic solvent in paints, shellacs, cosmetics, glues, inks, and other products. Prolonged exposure to toluene gas can seriously harm the central nervous system, liver, eyes, kidneys, lungs, and other organs.[12,13] The World Health Organization (WHO) recommends that the concentration of toluene in the environment used for everyday production must be less than 0.26 ppm (1 mg/m^3) in 30 min average and not more than 0.002 ppm (7.5 μg/m^3) in an annual mean. As the American Conference of Governmental Industrial Hygienists (ACGIH) suggests, an 8 h time-weighted average of 20 ppm is the

Received: February 27, 2024
Revised: April 22, 2024
Accepted: April 29, 2024

© XXXX American Chemical Society

threshold limit value for toluene. Furthermore, in accordance with the Occupational Safety and Health Administration (OSHA), toluene concentrations above 500 ppm may damage the central nervous system and other essential organs.[14] Hence, real-time monitoring of toluene gas at very low concentrations is of great importance for environmental monitoring and medicinal investigation.

Usually, metal oxide semiconductors (MOSs) like NiO, ZnO, SnO_2, WO_3, Fe_2O_3, etc., have been extensively used to recognize toluene owing to their small dimensions, low cost, good precision and simple fabrication.[15−17] For instance, Singh et al. fabricated the Al doped NiO sensor, which was able to detect 10 ppm toluene gas. The sensor showed the response of 29 at an elevated temperature of 180 °C.[18] Wang et al. prepared the Fe-doped NiO based toluene sensor at 212.5 °C where this sensor exhibited a response of 36 toward 100 ppm toluene.[19] Lee et al. reported the Au coated SnO_2 nanorod array based toluene sensor, which revealed a response toward 10 ppm toluene at an operating temperature of 450 °C.[20] David et al. described the Ag/Bi_2O_3 nanocomposite based RT toluene gas sensor, which was able to detect 10 ppm toluene gas. The sensor displayed a response of 89.2% toward 50 ppm toluene gas. The sensor was fabricated on the surface of a ceramic plate and response and recovery time was not clearly mentioned.[21] Suematsu et al. reported the SnO_2 nanoparticle-based toluene gas sensor which revealed the response of 40 at a high temperature of 400 °C. The important parameters such as detection limit, relative humidity (RH), response time, and recovery time of this sensor were nether investigated nor calculated.[22] Tshabalala et al. prepared the TiO_2 nanowires and flowerlike hierarchical structure-based toluene gas sensor, which was able to detect 40 ppm toluene gas. This sensor showed a response of 6.57 toward 40 ppm toluene at an operating temperature of 25 °C. The sensor showed a quite high response time of 120 s.[23] However, these MOS sensors require high working temperatures and cannot be employed in flexible systems since the flexible sensors cannot function at higher temperatures. Hence, it is imperative to develop a new sensing material that can identify the target gas at RT and uses less power.

The discovery of MXenes in 2011 has set a significant new milestone in the field of two-dimensional (2D) materials. MXenes, a new class of 2D layered transition metal carbides and nitrides, and used in different applications like gas sensing, supercapacitors, biosensors, batteries, etc., owing to their appetizing properties such as high electronic conductivity, unique layer morphology, large specific surface area, abundant absorption sites, different electronic properties, hydrophilic surfaces, and biocompatibility.[24−27] MXenes are prepared from the MAX phase and are represented as $M_{n+1}AX_n$, where M is an early transition metal (Ti, V, Cr, Mn, Zr, Nb, Mo, Ta, etc.), A is an element of group 13−15 of the periodic table (Al, Ga, In, Si, Ge, As, Sn, Pb, etc.), and X is carbon, nitrogen, or boron atoms. MXenes are developed after selective chemical etching of covalent bond A from the MAX phase and give a formula as $M_{n+1}XnTx$, where T denotes the surface termination groups such as −F, −Cl, −OH, −O, etc. Several theoretically predicted MXenes, such as Ti_3C_2, Ti_2C, Nb_2C, Mo_2C, V_2C, etc., have been successfully synthesized.[28]

Currently, a Ti_3C_2 MXene has been commonly used to detect various hazardous gases such as NO_2,[29] NH_3,[30] H_2S,[31] HCHO,[32] etc. at RT. The primary obstacles to using Ti_3C_2 in gas sensing applications are its small band gap and restacking tendency.[33] To solve these problems, in the current work, the vanadium carbide (V_2C) MXene has been used as a sensing material due to its lightweight, good electrical conductivity, and mechanical strength. V_2C is one of the nanomaterials in the MXenes family that comprises two M layers and one C layer, whereas Ti_3C_2 accommodates three Ti layers and two C layers. Moreover, V_2C possesses a thin atomic layer which stimulates the adsorption and desorption of analytes on the sensing materials.[34,35]

To the authors' knowledge, this is the first report on the V_2C MXene based flexible RT toluene gas sensor. The polyester film based transparent sheet was used to fabricate the flexible sensor. This work focuses on the HF etched route for V_2C MXene, its characterization, and analysis of the gas sensing behavior at RT. The sensor exhibited excellent selectivity, high response, and low detection limit toward the toluene gas.

2. EXPERIMENTAL SECTION

2.1. Materials and Methods. Vanadium pentoxide (V_2O_5, extra pure AR, 99.5%) and aluminum (Al) metal powder (Al, 99%, ∼325 mesh) were purchased from SRL Chemicals. Hydrofluoric acid (40%) was obtained from Avra Synthesis Private Limited, and carbon black (C) was procured from Sigma-Aldrich. Hydrochloric acid (extrapure) was obtained from Finar Chemicals.

2.2. Preparation of the V_2C MXene. The V_2C MXene was synthesized by using the HF etching route. Initially, a mixture of powders with a molar ratio of V_2O_5:Al:C = 1:4.63:1 was mixed using a mortar and pestle for 60 min. Then, the sample was made into pellets by using a press and placed in a tubular furnace at 1150 °C for 3 h under an Ar atmosphere. Here, the optimization of reaction temperature for V_2C MXene synthesis at 1150 °C was chosen based on a thorough understanding of the thermodynamic and kinetic processes involved, particularly considering the behavior of MAX phases. MAX phases begin forming at around 1000 °C, initiating the transformation into MXenes. However, the highest yield of MXenes is typically achieved between 1300 and 1400 °C. Beyond this optimal range, the degradation of MAX phases occurs, leading to the formation of carbides or nitrides, which can contaminate the MXene product.[36] At 1150 °C, the kinetics of the reaction remains favorable for conversion, while the risk of significant degradation and byproduct formation is reduced compared to higher temperatures. Therefore, the selection of 1150 °C as the optimized reaction temperature ensures a high yield of pure V_2C MXene product while maintaining operational feasibility and minimizing contamination. After this process, the sample was cooled down to RT, and it was ground into fine powder using a mortar and pestle. The obtained MAX powder was subsequently washed with 9 M HCl. The material was then neutralized using vacuum filtration and dried at 80 °C for 6 h. After that, the mixture was mixed with the etchant and stirred at 400 rpm for 24 h. The etchant (20 mL for 1 g of the sample) was a 6:3:1 mixture (by volume) of 12 M HCl, DI water, and 40 wt % HF. The solution was then placed into an autoclave reactor for 120 h at 90 °C in a hot air oven. After the mixture cooled, the impurities were removed from the resultant solution by repeatedly washing it with deionized water, alcohol, and diluted HCl until pH reached 7. Finally, the samples were dried at 80 °C to obtain the final V_2C MXene.

2.3. Materials Characterization. Using a JEOL JEM 3200FS transmission electron microscope and a Carl Zeiss Gemini 300 field emission scanning electron microscope (FESEM), the surface morphologies of the V_2C MXene were examined (TEM). Fourier transform infrared (FTIR) spectroscopy (model: IR Affinity spectrophotometer, spectral range: 500−4000 cm^{-1}) was used to analyze the surface functional groups in the sample. Using a Witec Alpha 300 confocal Raman microscope (model: λ = 532 nm; spectral range: 200−800 cm^{-1}), the chemical bonding and molecular system state were investigated. X-ray photoelectron spectroscopy (XPS) was used to analyze the elemental compositions, bonding, and oxidation states of the sample. For XPS measurements, the PHI 5000 versa

https://doi.org/10.1021/acsaelm.4c00369
ACS Appl. Electron. Mater. XXXX, XXX, XXX−XXX

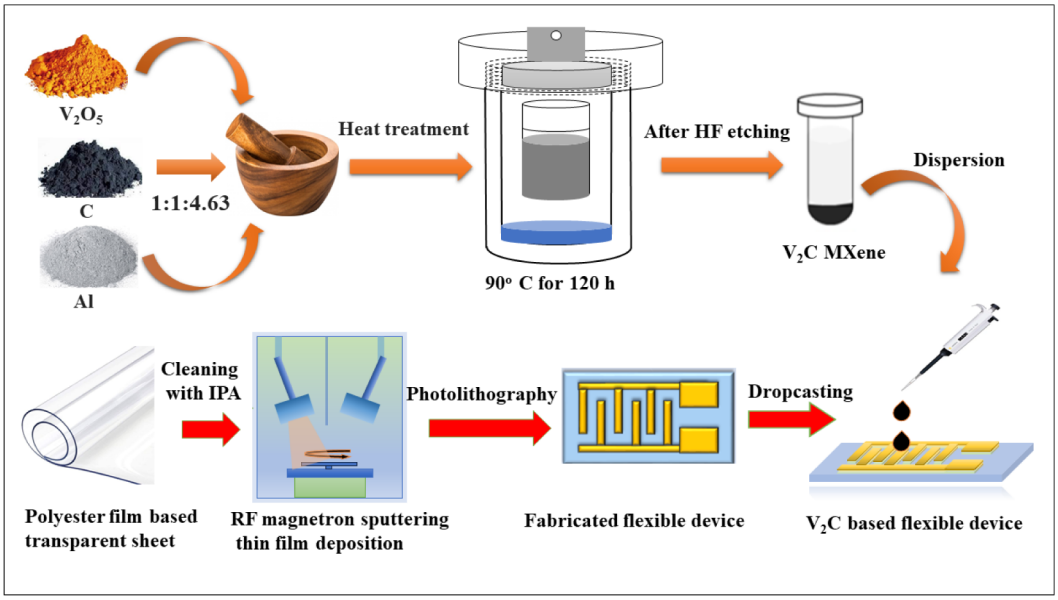

Figure 1. Fabrication steps of the V_2C MXene based flexible gas sensing device for RT toluene sensing.

probe III instrument and for characterization an Al Kα monochromatic X-ray source (1486.6 eV) were used.

2.4. Preparation of VOCs. Liquid organic compounds were put into a glass bubbler to produce VOC vapors. To generate the VOC vapors, dry air was exposed to the bubblers filled with liquid. After passing through an MFC with a limit of 10 sccm, the vapors were further diluted with dry air (passed through an MFC of 10 slpm). The dilution level could be precisely controlled via the two MFCs, and the resulting vapor was then injected into the gas chamber. Gas sensing setup can be found in Figure S1.

2.5. Device Fabrication. The flexible substrate (10 mm × 10 mm) was manufactured by using a polyester film based transparent sheet. Figure 1 depicts the fabrication procedure of the V_2C MXene based flexible toluene gas sensing device. At first, isopropyl alcohol (IPA) was used to clean the substrate. Thermal treatment of the transparent sheet was done at 80 °C to confirm its durability in the photolithography process. A 10 nm-thick chromium interlayer was applied to the sheet to enhance the quality of the gold's adherence. RF-sputtering was used to deposit a 200 nm thick gold layer on the substrate. Finally, photolithography was utilized to produce IDEs. The width and interdigit gap of the electrode were approximately 10 μm. After that, an aqueous V_2C MXene homogeneous solution was dropcast onto the flexible substrate and dried at 60 °C in a vacuum oven for 1 h to produce a uniform film thickness.

3. RESULTS AND DISCUSSIONS

3.1. FESEM and TEM Analyses. The morphological characteristics of the V_2C MXene sample were confirmed by FESEM analyses. A typical accordion-like multilayered structure of the V_2C MXene, with an average size of approximately 0.5−2 μm, is depicted in Figure 2a,b. The visible gap between V_2C MXene nanosheets in the high magnification FESEM micrograph (Figure 2c) indicates that the Al was entirely etched out of the sample, thus, allowing the toluene gas molecules to diffuse more easily. Moreover, the nanosheets are curved and interconnected with each other.

To further confirm the morphologies of the V_2C MXene, TEM analysis was carried out. From Figure 3a, the hierarchical structure of V_2C MXene is clearly witnessed. Numerous single V−C−V layers are placed on top of each other to form the layered structure (Figure 3b). The selected area diffraction pattern (SAED), characterized by spot patterns, confirms the

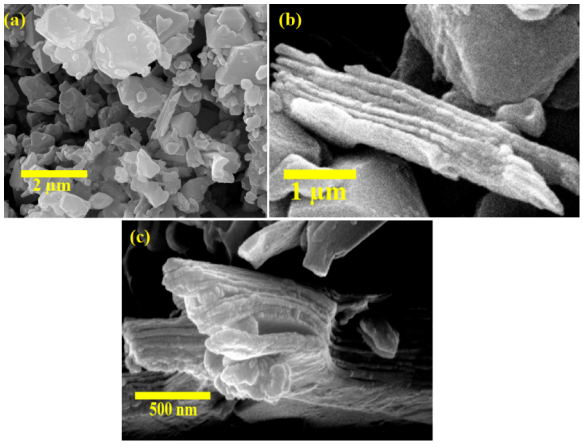

Figure 2. FESEM micrographs of the V_2C MXene at (a,b) low and (c) high magnification.

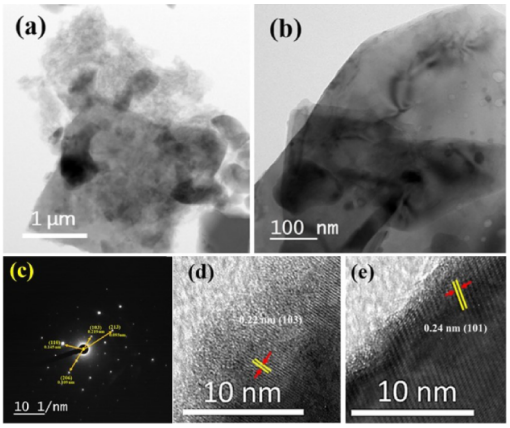

Figure 3. TEM micrographs at (a,b) low magnification and (c) SAED pattern; (d,e) HRTEM lattice fringes of the V_2C MXene sample.

crystalline nature of the sample. From the spot pattern, the identified crystallographic planes are (103), (110), (206), and (213) respectively, as depicted in Figure 3c. The HRTEM

https://doi.org/10.1021/acsaelm.4c00369
ACS Appl. Electron. Mater. XXXX, XXX, XXX−XXX

lattice fringe pattern (presented in Figure 3d,e) has interplanar spacings of 0.22 and 0.24 nm corresponding to the (103) and (101) planes of V_2C which maps well with the JCPDS Card # 00-029-0101 as well as with the literature.[37]

3.2. Raman, FTIR & XPS Analyses. Figure 4a displays the Raman spectrum of V_2C MXene. The presence of the peak at

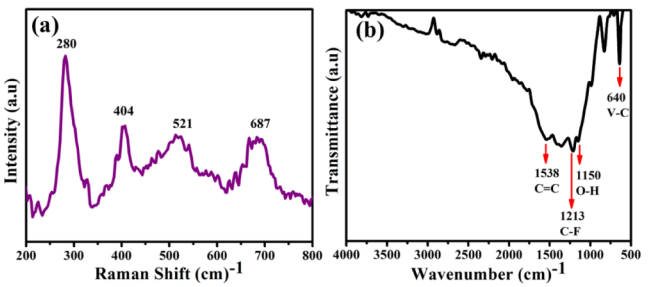

Figure 4. (a) Raman spectrum and (b) FTIR spectrum of V_2C MXene.

280 cm^{-1} is ascribed to the E_{1g} vibration mode, which further confirms the enhancive interlayer spading in V_2C MXene. The other three peaks located at 404, 521, and 687 cm^{-1} are attributed to the active vibration modes of the terminated V_2C. The presence of peaks at 280, 404, 521, and 687 cm^{-1} further ensures the elimination of the Al element from the MAX phase.[25] The peak at 404 cm^{-1} originates from the $V_2C(OH)_2$, whereas the peaks at 521 and 687 cm^{-1} are attributed to the A_1g vibrational modes of V_2CF_2 and $V_2CO(OH)$, respectively, based on the theoretical computation. The out-of-plane vibration and the in-plane vibration of V atoms are attributed to the A_{1g} and E_g modes, respectively.[38] Thus, this Raman analysis confirms the presence of surface functional groups −O, −F, and −OH in the V2C MXene. Furthermore, the FTIR analysis was performed to ascertain the chemical compositions of the V_2C MXene, as illustrated in Figure 4b. The peaks at 1538 and 640 cm^{-1} are due to the presence of C═C and V−C bands. The vibrational peaks appearing at 1213 and 1150 cm^{-1} confirm the presence of C−F and O−H bands, which further approves rich oxygen and fluorine containing functional groups. The FTIR spectrum validates the presence of V−C, O−H, C−F, and C═C bands.[39,40]

To obtain better insight into the chemical compositions and bonding of the V_2C MXene, XPS analyses were carried out. Figure 5a displays the survey spectrum of the V_2C MXene sample which confirms the presence of elements C, O, and V. In the high resolution V 2p spectrum (Figure 5b) two doublets were found wherein the peak appeared at 516.91 and 523.63 eV, 517.97 and 524.83 eV, and 519.07 and 525.93 eV are ascribed to V−C and V−O bonds. The formation of V−O is unavoidable after the removal of Al from the V_2AlC during the high temperature etching steps. It is because of the fact that MXene species are partly terminated with the oxygen functional groups. The presence of high intensity V−O bond is attributed to the fact that XPS primarily identifies the surface structure of samples.[25] The deconvoluted O 1s spectrum (Figure 5c) for the V_2C are fitted into three peaks at the binding energies of 530.44, 532.11, and 533.22 eV which correspond to V−C−O, V−O, and O−H bonds, respectively. The C 1s spectrum in Figure 5d is deconvoluted into four peaks at 283.40, 284.41, 285.85, and 288.01 eV, corresponding to C−V, C−C, C−O, and O−C═O bonds, respectively. Furthermore, to measure the bandgap of the as-synthesized

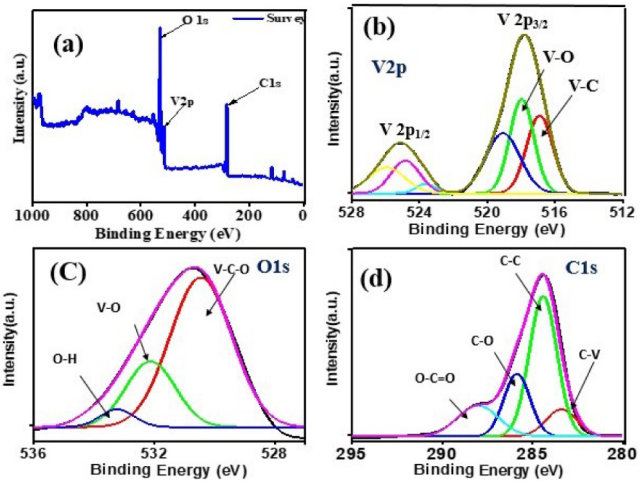

Figure 5. (a) Survey spectrum of V_2C MXene; XPS spectra for (b) V 2p, (c) O 1s, and (d) C 1s.

V_2C MXene, UV−visible spectroscopy was performed. Detailed Tauc's plot can be found in Figure S2.

3.3. RT Toluene Sensing. The excellent electrical conductivity, various functional groups, and the lightweight and biocompatibility of V_2C MXene have made them useful as a sensing material for flexible toluene detection at RT. The V_2C MXene based device was fabricated on a polyester film based transparent sheet substrate and its gas sensing characteristics were performed at RT (27 ± 1 °C). To investigate the sensing performance of the V_2C MXene-based flexible gas sensor, the device was exposed to toluene gas. The sensor response was calculated with the help of eq 1.

$$R_{response}(\%) = \frac{R_g - R_0}{R_0} \times 100 \quad (1)$$

where R_g = resistance of the sensor when NH_3 gas is exposed; R_0 = resistance of the sensor in air.

Figure 6a depicts the transient response of the V_2C MXene sensor examined at different concentrations of toluene gas ranging from 5 to 200 ppm. The sensor's response rises as the concentrations of toluene gas increase due to the presence of oxygen-containing functional groups such as hydroxyl (−OH) on the surface of V_2C. Figure 6b exhibits the calibration plot of the RT toluene sensor. In the concentration regime of 5−200 ppm, the sensor displays good linearity (R^2 = 0.9843). The limit of detection (LOD) was calculated using eq 2.

$$LOD = \frac{3\sigma}{s} \quad (2)$$

where, σ = the standard deviation and s = the slope of the calibration curve. The LOD of the V_2C based flexible gas sensor is determined to be 47.85 ppb at RT.

The response and recovery times of the accordion-like V_2C MXene based flexible sensor for 50 ppm toluene gas at RT are illustrated in Figure 6c. The response time is defined as the time required to reach 90% of its maximum value from 10% of the minimum value when gas is on, and the recovery time is the time required to reach 10% of the value from 90% when air is off. The calculated response and recovery values of the sensor are 14 and 34 s, respectively. The hump in recovery appears in almost every transient during the experiments. There may be possibly two reasons that induces this hump: (i)

https://doi.org/10.1021/acsaelm.4c00369
ACS Appl. Electron. Mater. XXXX, XXX, XXX−XXX

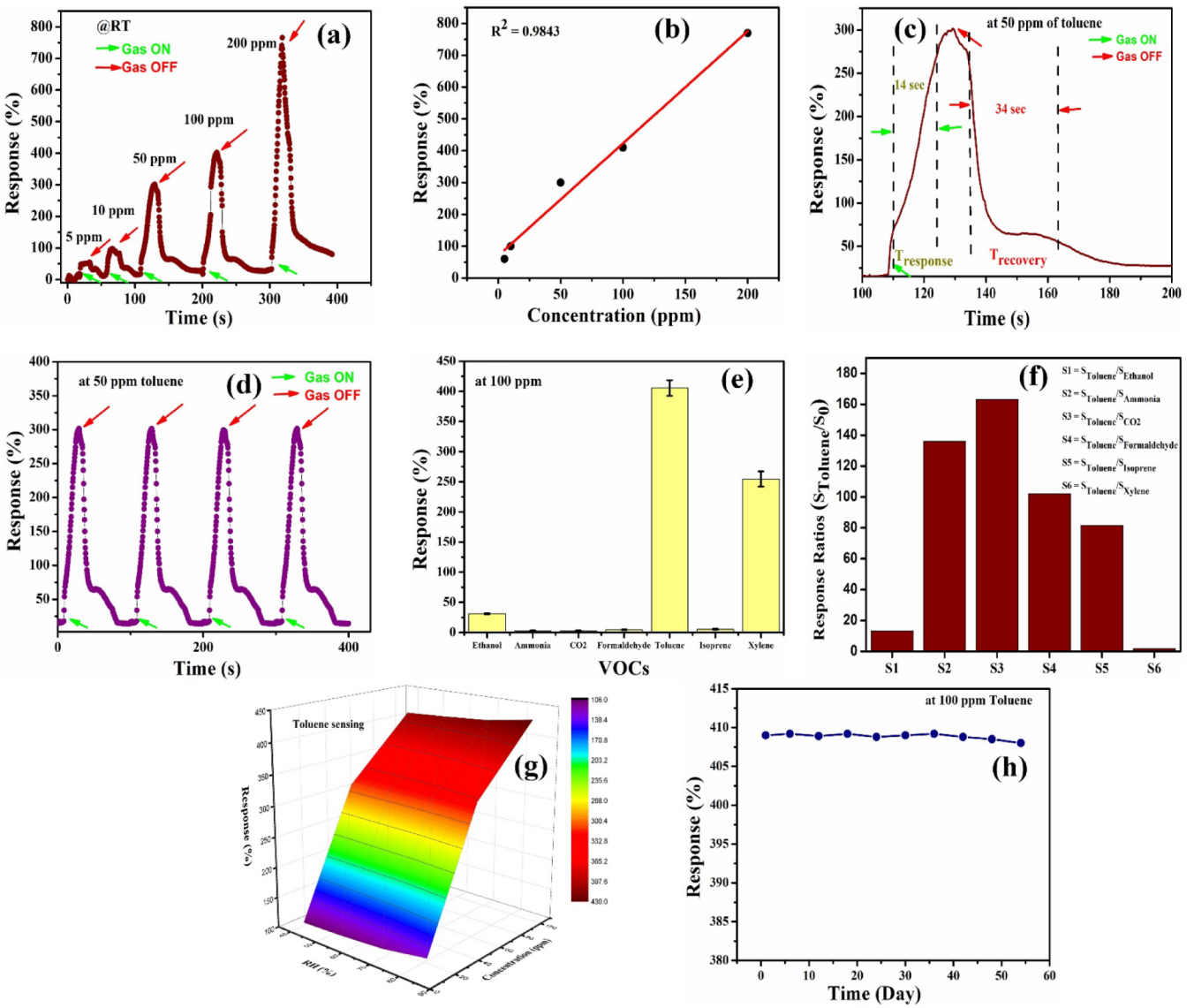

Figure 6. (a) Transient response of the V_2C MXene based flexible and RT (27 ± 1 °C) sensor toward different toluene concentrations over the range of 5−200 ppm; (b) calibration plot of the sensor at RT; (c) the response and recovery times of the device at 50 ppm toluene gas; (d) repeatability of the sensing device at 50 ppm toluene gas; (e) selectivity of the sensor under the exposure of different gases at 100 ppm; (f) cross-selectivity plot of toluene over other interfering gases; (g) effect of humidity on the toluene sensing behavior of the V_2C MXene based flexible RT sensor; (h) the stability plot of this sensor toward 100 ppm toluene.

there may be slight leakage in the gas sensing system, due to which the residual gases are adsorbed during the recovery period; (ii) it may also be a property of the sensor that it encompasses some reorientation in its atomic arrangement during recovery. However, in both the cases the response is consistent with different gases in different concentrations. Hence, this illustrates the stable nature of the sensor. These fast response and recovery values of the sensor are attributed to the accordion-like morphology of the surface and more number of active sites. The quick sensing response of the V_2C MXene-based sensor ensured real-time monitoring of toluene gas at RT.

The reproducibility of the sensor was assessed by exposing the sensing material to the target gas and air consequently. Figure 6d shows the reproducibility of the V_2C MXene based on 50 ppm toluene gas at RT. The sensor was exposed to four consecutive cycles of toluene vapors. It is evident that all of the response and recovery values reach their baseline when the target gas is turned on and off, respectively. Furthermore, there is no significant baseline drift in the response of the sensor, demonstrating its good reproducibility.

Selectivity is one of the crucial parameters in a gas sensor due to its industrial application. Figure 6e demonstrates the selectivity plot with the error bars of the V_2C MXene-based sensor toward ethanol, ammonia, carbon dioxide, formaldehyde, toluene, isoprene, and xylene at the same concentration of 100 ppm at RT. The sensor shows an excellent response (408%) at 100 ppm toluene, which was 12.8, 136, 163, 102, 81.6, and 1.59 times higher than the ethanol, ammonia, carbon dioxide, formaldehyde, isoprene, and xylene gases, respectively. we received approximately 256% response toward 100 ppm xylene gases due to similar molecular structure of xylene. The brilliant selectivity toward toluene over six other hazardous gases is attained because of the comparatively weak interaction and adsorption of the interfering gases with the sensing material. The presence of

https://doi.org/10.1021/acsaelm.4c00369
ACS Appl. Electron. Mater. XXXX, XXX, XXX−XXX

enormous functional groups in the sensing material leads to a high degree of selectivity toward toluene vapor molecules. To assess the cross-selectivity of the V_2C MXene based flexible sensors, the selectivity coefficient (K) was determined using the equation, $K = S_{toluene}/S_0$ where, $S_{toluene}$ signifies the response of the sensor, and S_0 represents response of the other interfering gases like ethanol, ammonia, carbon dioxide, formaldehyde, isoprene and xylene. Figure 6f illustrates the cross-selectivity values toward toluene over other gases, indicating that all cross-selectivity values are greater than 1.5. This data signify good cross-selectivity of the V_2C MXene based RT toluene sensor.[41] To further investigate the effect of humidity on sensing, the sensor was exposed to different RH values as shown in Figure 6g. It is observed that the sensor exhibits stable response in the presence of humidity; however at a higher humid environment, the response slightly deviates from the mean response due to proton hopping (Grotthuss mechanism). The stability of the sensor was assessed by storing it under an ambient atmosphere for a period of 50 days. Figure 6h exhibits the stability plot of this sensor toward 100 ppm toluene. It reveals a stable performance of this flexible sensor for 50 days, after which its shows a slight decrease in response. This decrease may be attributed to the adsorption of the atmospheric gases on the surface of the V_2C MXene based sensor. Detailed resistance and response plots of the sensors can be found in Figures S3 and S4.

3.4. Sensing Mechanism. When the target gas, toluene, is exposed to the V_2C based flexible RT sensor, the toluene gas molecules react with the various functional groups (−OH, −F, −O) of V_2C to form a surface bond. As a result, the conducting channel in the V_2C MXene is impeded, which increases the sensor's resistance, thus revealing the p-type behavior of the V_2C. When the V_2C MXene interacts with air (O_2), electrons are extracted from the conduction band of the sensing material and the hole accumulation layer (HAL) is formed near the grain boundaries, thus increasing the carrier concentrations. These changes increase the conductivity of the gas sensor, as holes are the majority carriers in the sensing material. When the sensor is exposed to toluene vapors, these electrons are released back to the conduction band of V_2C MXene and recombined with the holes. This leads to a reduction in the concentrations of holes, thereby increasing the resistance of the sensor. The functional groups like −O, −OH, and −F are present on the surface of the V_2C MXene (FTIR XPS and Raman spectra). In the presence of toluene gas, the V_2C MXene interacts with the toluene gas molecules through the -F functional groups, and these F groups attach with the *ortho*, *meta*, or para position of the toluene vapors as illustrated in Figure 7. This interaction causes the charge transfer between the sensing layer and toluene vapor, thus leading to a change in the values of the resistances.

The electron donating nature of the toluene vapors induces charge transfer to the sensing material via the −F links. This reduces the majority hole concentration of the V_2C MXene sensing layer and thereby elevating the resistance of the sensing device.

The sensing mechanism can be explained using the Kroger−Vink notation. The p-type nature of the V_2C MXene can be attributed to two possible mechanisms within the crystal lattice. Cationic deficiency is a probable mechanism through which excess positive charges are induced in the crystal, making it p-type. The cationic deficiency can be depicted as illustrated in eq 3:

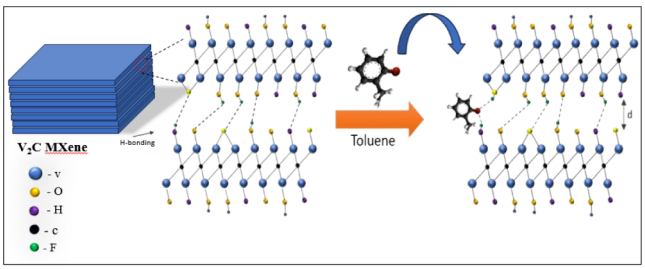

Figure 7. Gas sensing mechanism of the V_2C MXene based RT toluene sensor.

$$V'_A + h^* + X_X^X \rightarrow 1/2\ X_2 \quad (3)$$

where, V'_A represents cationic vacancy with a negative charge, and h* represents positively charged holes. A represents the cations/metallic ions, and X represents the anions in the crystal. X_X^X represents the anions located in its own position and hence carrying no charge.

Excess anions at the interstitial sites majorly contribute to the p-type behavior of the V_2C MXene. The anionic interstitials can be represented in eq 4 as illustrated below:

$$A_A^X + X_X^X \rightarrow A_A^X + X_i' + h^* \quad (4)$$

A_A^X represents the cations located in its own position and hence carrying no charge. X_i' represents the anionic interstitials carrying negative charges, and h* represents positively charged holes.

In the presence of air, the oxygen molecules from the ambience interact with the sensing layer by capturing electrons and inducing more holes in the sensing layer. This reduces the resistance of the sensing layer. When the sensor is exposed to toluene, the toluene vapor binds with the sensing layer through the −F links, electron transfer takes place from the toluene molecule to the sensing layer. The holes, h* from (eqs 3 and 4 recombines with the incoming electrons from toluene and its reduction induces an enhancement in the values of resistances of the sensing layer. The change in the values of the resistances is demonstrated as the response of the sensing layer. In presence of air, the oxygen molecules from the ambience interacts with the sensing layer by capturing electrons and inducing more holes in the sensing layer. This reduces the resistance of the sensing layer. When the sensor is exposed to toluene, the toluene vapor binds with the sensing layer through the −F links, and electron transfer takes place from the toluene molecule to the sensing layer.

As per the authors' knowledge, no reports are available in the literature based on the V_2C MXene based flexible and RT toluene gas sensor. However, to assess the analytical performances of our developed gas sensing device, this flexible sensor has also been compared with the other 2D material-based toluene gas sensors, as illustrated in Table I. The majority of these works either discuss the use of rigid substrate and composite materials or doping with additional noble metals to attain better sensing performance or identify the target gas (here, toluene) at elevated temperatures. But here, the V_2C MXene based flexible sensor was fabricated to detect toluene gas at RT, which reveals various advantages like huge response of 775% at 200 ppm, low LOD, shorter response and recovery times, and high selectivity. Therefore, this V_2C

https://doi.org/10.1021/acsaelm.4c00369
ACS Appl. Electron. Mater. XXXX, XXX, XXX−XXX

Table I. Comparison in Performance of the V_2C MXene Based Toluene Gas Sensor at RT with Other Reported 2D Material-Based Toluene Sensors[a]

sensing material	operating temperature (°C)	concentration (ppm)	LOD	cross-selectivity	response/ recovery time (s)	response	substrate	ref
Ag NPs/g-C_3N_4	200	50	NA	NA	28/24	25.4	copper film	42
g-C_3N_4/Co_3O_4	220	100	NA	NA	83/-	17.02	-	43
V_2O_5/GO	RT	60	2.12	$S_{toluene}/S_{methanol}$ = 3.28	12.68/14.53	36.25	ITO coated glass	44
MoS_2 (W)	RT	100	NA	NA	52/50	12.5%	silica glass	45
RGO/PEO	RT	100	NA	NA	219/165	0.04	SiO_2 film	46
CuO/$Ti_3C_2T_x$ MXene	250	50	0.32 ppm	$S_{toluene}/S_{ethanol}$ = 1.64	270/10	11.4	silicate glass	47
Mo_2CT_X	RT	100	220 ppb	$S_{toluene}/S_{benzene}$ = 1.64		2.65%	Si/SiO_2	48
V_2C MXene	RT	200	47 ppb	$S_{toluene}/S_{ethanol}$= 13.16	14/34	775%	polyester film based flexible transparent sheet	this work

[a]Ag = gold; NPs = nanoparticles; g-C_3N_4 = graphitic carbon nitride; Co_3O_4 = cobalt oxide; NWs = nanowires: V_2O_5 = vanadium pentoxide; GO = graphene oxide; MoS_2 (W) = molybdenum sulfide (water); RGO = reduced graphene oxide; PEO = poly(ethylene oxide); CuO = copper monoxide; $Ti_3C_2T_x$ = titanium carbide.

MXene based flexible and RT toluene gas sensor is favorable for industrial applications.

4. CONCLUSION

Here, a RT (27 ± 1 °C) flexible toluene gas sensor using the V_2C MXene with the band gap of 3.9 eV was effectively developed. On the V_2C MXene-based sensor surface, the layered structure makes gas adsorption easier. The gas sensing mechanism as well as the impact of humidity of this flexible sensor toward toluene vapors have been thoroughly described. This sensor showed an excellent selectivity toward toluene over six other hazardous gases, a low detection limit of 47.85 ppb, good reproducibility, cross-selectivity, long-term stability of 50 days, and short response and recovery times of 14 and 34 s, respectively, with an excellent response of 775% at 200 ppm toluene. The sensor operates linearly over 5−200 ppm toluene gas. Thus, our fabricated RT toluene gas sensor will open up new possibilities for the development of cutting-edge materials and devices for the future generation of wearable electronics.

■ ASSOCIATED CONTENT

Supporting Information

The Supporting Information is available free of charge at https://pubs.acs.org/doi/10.1021/acsaelm.4c00369.

Schematic of the gas sensing setup, Tauc's plot of V_2C MXene, response of the V_2C MXene based flexible and RT sensor toward toluene gas at 500 ppb, and resistance plots of the sensors toward different interfering gases (PDF)

■ AUTHOR INFORMATION

Corresponding Authors

Rinky Sha − *Sensors for Health-Care and Environmental Monitoring (SHE) Lab, Department of Electronics and Communication Engineering, Indian Institute of Information Technology Kalyani, West, Bengal 741235, India;* orcid.org/0000-0002-5175-3059; Email: rinky@iiitkalyani.ac.in

Sushmee Badhulika − *Department of Electrical Engineering, Indian Institute of Technology, Hyderabad 502285, India;* Email: sbadh@ee.iith.ac.in

Authors

Sourav Karmakar − *Sensors for Health-Care and Environmental Monitoring (SHE) Lab, Department of Electronics and Communication Engineering, Indian Institute of Information Technology Kalyani, West, Bengal 741235, India;* orcid.org/0000-0003-2825-1234

Mavuri Sai Deepak − *Department of Electrical Engineering, Indian Institute of Technology, Hyderabad 502285, India*

Om Priya Nanda − *Department of Electrical Engineering, Indian Institute of Technology, Hyderabad 502285, India*

Avik Sett − *Department of Microelectronics, Delft University of Technology (TU Delft), Delft 2628 CD, Netherlands;* orcid.org/0000-0001-8437-607X

Palash Chandra Maity − *Department of Materials Engineering, Indian Institute of Science, Bangalore 560012, India*

Gairik Karmakar − *Department of Electronics and Electrical Communications Engineering, Indian Institute of Technology Kharagpur, West, Bengal 721302, India*

Tarun Kanti Bhattacharyya − *Department of Electronics and Electrical Communications Engineering, Indian Institute of Technology Kharagpur, West, Bengal 721302, India;* orcid.org/0000-0002-7699-6436

Complete contact information is available at: https://pubs.acs.org/10.1021/acsaelm.4c00369

Author Contributions

S.K., M.S.D., O.P.N., A.S., P.C.M., and G.K. contributed to research, methodology, data curation, data compilation, investigation, writing − original draft, preparation, and writing − review and editing. R.S. contributed to supervision, conceptualization, resources, project administration, and writing − review and editing. S.B. and T.K.B. contributed to conceptualization and writing − review and editing.

Notes

The authors declare no competing financial interest.

■ REFERENCES

(1) Karmakar, S.; Sett, A.; Maity, P. C.; Karmakar, G.; Sha, R.; Bhattacharyya, T. K.; Lahiri, I. A room-temperature gas sensor based on 2D Ni−Co−Zn ternary oxide nanoflakes for selective and sensitive ammonia detection. *Dalton Trans.* **2023**, *52* (44), 16500−16512.

(2) Fang, B.; Yao, H.; Xiao, X.; Zhang, Q.; Zhang, X.; Yang, W. Metal-organic frameworks-derived hollow Co3O4 nanotubes for efficient detection of toluene vapor. *J. Alloys Compd.* **2023**, *937*, 168535.
(3) Bag, A.; Lee, N. E. Recent advancements in development of wearable gas sensors. *Adv. Mater. Technol.* **2021**, *6* (3), 2000883.
(4) Tian, X.; Cui, X.; Xiao, Y.; Chen, T.; Xiao, X.; Wang, Y. Pt/MoS2/Polyaniline Nanocomposite as a Highly Effective Room Temperature Flexible Gas Sensor for Ammonia Detection. *ACS Appl. Mater. Interfaces* **2023**, *15* (7), 9604−9617.
(5) Yang, Z.; Jiang, L.; Wang, J.; Liu, F.; He, J.; Liu, A.; Lv, S.; You, R.; Yan, X.; Sun, P.; et al. Flexible resistive NO2 gas sensor of three-dimensional crumpled MXene $Ti_3C_2T_x$/ZnO spheres for room temperature application. *Sens. Actuators, B* **2021**, *326*, 128828.
(6) Quan, W.; Shi, J.; Luo, H.; Fan, C.; Lv, W.; Chen, X.; Zeng, M.; Yang, J.; Hu, N.; Su, Y.; et al. Fully Flexible MXene-based Gas Sensor on Paper for Highly Sensitive Room-Temperature Nitrogen Dioxide Detection. *ACS Sens.* **2023**, *8* (1), 103−113.
(7) Lawaniya, S. D.; Kumar, S.; Yu, Y.; Awasthi, K. Flexible, Low-Cost, and Room Temperature Ammonia Sensor Based on Polypyrrole and Functionalized MWCNT Nanocomposites in Extreme Bending Conditions. *ACS Appl. Polym. Mater.* **2023**, *5* (3), 1945−1954.
(8) Kumar, A.; Kumar, A.; Varma, G. D. Flexible humidity-tolerant γ-Fe $_2O_3$-rGO-based nanohybrids for energy efficient selective NO_2 gas sensing. *New J. Chem.* **2023**, *47* (10), 4871−4879.
(9) Serpente, V.; Girolami, M.; Mastellone, M.; Sabbatella, G.; Vitulano, A.; Staccioli, M. P.; Riccucci, C.; Carlo, G. D.; Trucchi, D. M. Selective flexible sensor for monitoring volatile organic compounds in museum display cases. *J. Cult. Heritage* **2024**, *66*, 1−9.
(10) Manzoor, S.; Talib, M.; Arsenin, A. V.; Volkov, V. S.; Mishra, P. Polyethyleneimine-starch functionalization of single-walled carbon nanotubes for carbon dioxide sensing at room temperature. *ACS Omega* **2023**, *8* (1), 893−906.
(11) Manzoor, S.; Talib, M.; Novikov, S. M.; Arsenin, A. V.; Volkov, V. S.; Mishra, P. Physisorption-Mediated Charge Transfer in TiS_2 Nanodiscs: A Room Temperature Sensor for Highly Sensitive and Reversible Carbon Dioxide Detection. *ACS Sens.* **2023**, *8* (9), 3435−3447.
(12) Liu, H.; Wang, Z.; Sun, C.; Shao, J.; Li, Z.; Zhang, H.; Qiu, M.; Pan, G.; Yang, X. Construction of Co_3O_4/Fe_3O_4 heterojunctions from metal organic framework derivatives for high performance toluene sensor. *Sens. Actuators, B* **2023**, *375*, 132863.
(13) Min, S. K.; Kim, H. S.; Chang, S. P. Highly sensitive toluene sensor based on porous core-shell-structured In2O3−ZnO nanofibers under UV irradiation at room temperature. *Phys. E (Amsterdam, Neth.)* **2023**, *154*, 115806.
(14) Garg, G.; Garg, N.; Deep, A.; Soni, D. Zr-MOF and PEDOT:PSS composite sensor for chemoresistive sensing of toluene at room temperature. *J. Alloys Compd.* **2023**, *956*, 170309.
(15) Ji, H.; Liu, Y.; Zhang, R.; Yuan, Z.; Meng, F. Detection and recognition of toluene and butanone in mixture based on SnO2 sensor via dynamic transient and steady-state response analysis in jump heating voltage mode. *Sens. Actuators, B* **2023**, *376*, 132969.
(16) Mokoena, T. P.; Swart, H. C.; Nhlapo, T. A.; Mofokeng, S. J.; Malevu, T. D.; Mhlongo, M. R.; Motaung, D. E. Influence of exposure time and bias voltage on the response kinetics of toluene vapour on Ho^{3+}-doped NiO chemiresistive sensors: Yellow-emitter nano-phosphors. *Inorg. Chem. Commun.* **2023**, *158*, 111378.
(17) Karmakar, S.; Sett, A.; Maity, P. C.; Sha, R.; Bhattacharyya, T. K.; Lahiri, I. A highly selective room-temperature formaldehyde gas sensor based on vertically aligned 1D $NiCo_2O_4$ nanoneedles. *Mater. Lett.* **2023**, *350*, 134927.
(18) Shailja, S.; Singh, K.; Singh, R. C. Enhanced toluene sensing performance of nanostructured aluminium-doped nickel oxide gas sensor. *Appl. Phys. A* **2023**, *129* (4), 263.
(19) Wang, M.; Liu, H.; Sun, C.; Pan, G.; Yang, X.; Shao, J.; Dong, J.; Qi, Y. High efficiency toluene sensor based on iron-doped nickel oxide triple-shell microspheres with high moisture resistance. *Mater. Sci. Eng.* **2024**, *299*, 117001.
(20) Lee, J.; Min, H.; Choe, Y. S.; Lee, Y. G.; Kim, K.; Lee, H. S.; Lee, W. Highly sensitive and selective detection of benzene, toluene, xylene, and formaldehyde using Au-coated SnO_2 nanorod arrays for indoor air quality monitoring. *Sens. Actuators, B* **2023**, *394*, 134359.
(21) David, S. P.; Veeralakshmi, S.; Sandhya, J.; Nehru, S.; Kalaiselvam, S. Room temperature operatable high sensitive toluene gas sensor using chemiresistive Ag/Bi_2O_3 nanocomposite. *Sens. Actuators, B* **2020**, *320*, 128410.
(22) Suematsu, K.; Oyama, T.; Mizukami, W.; Hiroyama, Y.; Watanabe, K.; Shimanoe, K. Selective detection of toluene using pulse-driven SnO2 micro gas sensors. *ACS Appl. Electron. Mater.* **2020**, *2* (9), 2913−2920.
(23) Tshabalala, Z. P.; Mokoena, T. P.; Jozela, M.; Tshilongo, J.; Hillie, T. K.; Swart, H. C.; Motaung, D. E. TiO_2 nanowires for humidity-stable gas sensors for toluene and xylene. *ACS Appl. Nano Mater.* **2021**, *4* (1), 702−716.
(24) Yu, H.; Dai, L.; Liu, Y.; Zhou, Y.; Fan, P.; Luo, J.; Zhong, A. $Ti_3C_2T_x$ MXene-SnO_2 nanocomposite for superior room temperature ammonia gas sensor. *J. Alloys Compd.* **2023**, *962*, 171170.
(25) Guan, Y.; Jiang, S.; Cong, Y.; Wang, J.; Dong, Z.; Zhang, Q.; Yuan, G.; Li, Y.; Li, X. A hydrofluoric acid-free synthesis of 2D vanadium carbide (V_2C) MXene for supercapacitor electrodes. *2D Mater.* **2020**, *7* (2), 025010.
(26) Yang, G.; Liu, F.; Zhao, J.; Fu, L.; Gu, Y.; Qu, L.; Zhu, C.; Zhu, J.-J.; Lin, Y. MXenes-based nanomaterials for biosensing and biomedicine. *Coord. Chem. Rev.* **2023**, *479*, 215002.
(27) Cao, L. C. T.; Zhou, M. H.; Opaprakasit, P.; Sreearunothai, P.; Nagao, Y.; Boonruang, S.; Fallah, S. H.; Tseng, S.-F.; Hsu, S.-H. Facile Fabrication of Oxygen-Enriched MXene-Based Sensor and Their Ammonia Gas-Sensing Enhancement. *Adv. Mater. Interfaces* **2023**, *10* (16), 2300166.
(28) Gogotsi, Y. The Future of MXenes. *Chem. Mater.* **2023**, *35* (21), 8767−8770.
(29) Gasso, S.; Sohal, M. K.; Mahajan, A. MXene modulated SnO_2 gas sensor for ultra-responsive room-temperature detection of NO_2. *Sens. Actuators, B* **2022**, *357*, 131427.
(30) Pasupuleti, K. S.; Thomas, A. M.; Vidyasagar, D.; Rao, V. N.; Yoon, S. G.; Kim, Y. H.; Kim, S.-G.; Kim, M.-D. ZnO@ $Ti_3C_2T_x$ MXene Hybrid Composite-Based Schottky-Barrier-Coated SAW Sensor for Effective Detection of Sub-ppb-Level NH_3 at Room Temperature under UV Illumination. *ACS Mater. Lett.* **2023**, *5* (10), 2739−2746.
(31) Hosseini-Shokouh, S. H.; Zhou, J.; Berger, E.; Lv, Z. P.; Hong, X.; Virtanen, V.; Kordas, K.; Komsa, H.-P. Highly Selective H_2S Gas Sensor Based on $Ti_3C_2T_x$ MXene−Organic Composites. *ACS Appl. Mater. Interfaces* **2023**, *15* (5), 7063−7073.
(32) Niu, G.; Zhang, M.; Wu, B.; Zhuang, Y.; Ramachandran, R.; Zhao, C.; Wang, F. Nanocomposites of pre-oxidized $Ti_3C_2T_x$ MXene and SnO_2 nanosheets for highly sensitive and stable formaldehyde gas sensor. *Ceram. Int.* **2023**, *49* (2), 2583−2590.
(33) Soni, V.; Singh, P.; Quang, H. H. P.; Khan, A. A. P.; Bajpai, A.; Van Le, Q.; Thakur, V. K.; Thakur, S.; Nguyen, V.-H.; Raizada, P. Emerging architecture titanium carbide ($Ti_3C_2T_x$) MXene based photocatalyst toward degradation of hazardous pollutants: Recent progress and perspectives. *Chemosphere* **2022**, *293*, 133541.
(34) Wang, X.; Gong, L.; Li, Z.; Yin, Y.; Zhang, D. A room temperature ammonia gas sensor based on cerium oxide/MXene and self-powered by a freestanding-mode triboelectric nanogenerator and its multifunctional monitoring application. *J. Mater. Chem. A* **2023**, *11* (14), 7690−7701.
(35) Nanda, O. P.; Prince, A. G.; Durai, L.; Badhulika, S. Nickel MXene Nanosheet and Heteroatom Self-Doped Porous Carbon-Based Asymmetric Supercapacitors with Ultrahigh Energy Density. *Energy Fuels* **2023**, *37* (6), 4701−4710.
(36) Ud Din, M. F.; Yang, C.; Tang, Y.; Tian, Y.; Luo, Y.; Wu, Y.; Que, W. Efficient and cost-effective method to synthesize highly purified Ti_4AlN_3 and Ti_2AlN. *J. Adv. Dielect.* **2019**, *9* (1), 1950008.
(37) Majhi, S. M.; Ali, A.; Greish, Y. E.; El-Maghraby, H. F.; Mahmoud, S. T. V_2CT_X MXene-based hybrid sensor with high

https://doi.org/10.1021/acsaelm.4c00369
ACS Appl. Electron. Mater. XXXX, XXX, XXX−XXX

selectivity and ppb-level detection for acetone at room temperature. *Sci. Rep.* **2023**, *13* (1), 3114.
(38) Champagne, A.; Shi, L.; Ouisse, T.; Hackens, B.; Charlier, J. C. Electronic and vibrational properties of V_2C-based MXenes: From experiments to first-principles modeling. *Phys. Rev. B* **2018**, *97* (11), 115439.
(39) Zaka, A.; Mansoor, M. A.; Asghar, M. A.; Haider, A.; Iqbal, M. V_2C MXene-TiO_2 nanocomposite as an efficient electrode material for oxygen evolution reaction (OER). *Int. J. Hydrogen Energy* **2023**, *48* (89), 34599−34609.
(40) Kong, Y.; Li, Z.; Liu, Q.; Song, J.; Zhu, Y.; Lin, J.; Song, L.; Li, X. Artificial neural network-facilitated V_2C MNs-based colorimetric/fluorescence dual-channel biosensor for highly sensitive detection of AFB1 in peanut. *Talanta* **2024**, *266*, 125056.
(41) Makole, R.; Tshabalala, Z. P.; Swart, H. C.; Coetsee-Hugo, L.; Leshabane, N.; Motaung, D. E. Fabrication of one-dimensional porous p-type Co_3O_4 rods-based sensors for ultra-high sensitivity and selectivity towards benzene vapour. *Mater. Today Commun.* **2024**, *38*, 108426.
(42) Moradi, R.; Yousefi, R.; Adelpour, Z.; Sadeghi, M. The effects of Ag concentration on toluene gas sensing performance of Ag NPs decorated on g-C_3N_4 sheets. *J. Alloys Compd.* **2023**, *932*, 167539.
(43) Niu, J. Y.; Wang, L.; Xu, J. C.; Jin, H. X.; Hong, B.; Jin, D. F.; Peng, X. L.; Ge, H. L.; Wang, X. Q. Mesoporous Co_3O_4 nanowires decorated with g-C_3N_4 nanosheets for high performance toluene gas sensors based on p-n heterojunction. *Mater. Chem. Phys.* **2023**, *293*, 126980.
(44) Srivastava, S.; Singh, A.; Sahz, M. A.; Yadav, B. C.; Pandey, N. K. Development of V_2O_5@ GO (1D/2D) nanohybrid based chemiresistor for low-trace of toluene. *Sens. Actuators, B* **2024**, *400*, 134817.
(45) Taufik, A.; Asakura, Y.; Kato, H.; Kakihana, M.; Saleh, R.; Sekino, T.; Yin, S. 1T/2H-MoS_2 engineered by in-situ ethylene glycol intercalation for improved toluene sensing response at room temperature. *Adv. Powder Technol.* **2020**, *31* (5), 1868−1878.
(46) Su, Y.; Xie, G.; Chen, J.; Du, H.; Zhang, H.; Yuan, Z.; Ye, Z.; Du, X.; Tai, H.; Jiang, Y. Reduced graphene oxide−polyethylene oxide hybrid films for toluene sensing at room temperature. *RSC Adv.* **2016**, *6* (100), 97840−97847.
(47) Hermawan, A.; Zhang, B.; Taufik, A.; Asakura, Y.; Hasegawa, T.; Zhu, J.; Shi, P.; Yin, S. CuO nanoparticles/$Ti_3C_2T_x$ MXene hybrid nanocomposites for detection of toluene gas. *ACS Appl. Nano Mater.* **2020**, *3* (5), 4755−4766.
(48) Guo, W.; Surya, S. G.; Babar, V.; Ming, F.; Sharma, S.; Alshareef, H. N.; Schwingenschlögl, U.; Salama, K. N. Selective toluene detection with Mo_2CT_x MXene at room temperature. *ACS Appl. Mater. Interfaces* **2020**, *12* (51), 57218−57227.

https://doi.org/10.1021/acsaelm.4c00369
ACS Appl. Electron. Mater. XXXX, XXX, XXX−XXX